Nickel-Based Dye-Sensitized Photocathode: Towards Proton Reduction Using a Molecular Nickel Catalyst and an Organic Dye

van den Bosch, B.; Rombouts, J.A.; Orru, R.V.A.; Reek, J.N.H.; Detz, R.J.

DOI
10.1002/cctc.201600025

Publication date
2016

Document Version
Final published version

Published in
ChemCatChem

ChemPubSoc Europe

DOI: 10.1002/cctc.201600025

CHEMCATCHEM Full Papers

Nickel-Based Dye-Sensitized Photocathode: Towards Proton Reduction Using a Molecular Nickel Catalyst and an Organic Dye

Bart van den Bosch,[a] Jeroen A. Rombouts,[b] Romano V. A. Orru,[b] Joost N. H. Reek,*[a] and Remko J. Detz*[a]

To construct an efficient dye-sensitized photo-electrochemical tandem cell for hydrogen production, it is crucial to understand the working principles of both the photoanode and the photocathode. Herein, the anchoring of a proton-reduction catalyst and an organic dye molecule on metal oxides is studied for the preparation of a photocathode. On TiO_2, the Ni catalyst behaves as a good electrocatalyst ($-250\ \mu A\ cm^{-2}$) in acidic water (pH 2). The Ni catalyst and the organic dye were co-immobilized on NiO to form a solely Ni-based photocathode. The electron-transfer steps were investigated by using various techniques (IR, UV/Vis, and fluorescence spectroscopy, and (photo)electrochemistry). Despite the observed successful single-electron-transfer steps between all of the components, photocatalysis did not yield any hydrogen gas. Possible bottlenecks that prevent photocatalytic proton reduction are poor electron transfer because of aggregation, charge recombination from the catalyst to the NiO, or instability of the catalyst after the first reduction.

Introduction

The storage of solar energy as fuel by the light-driven splitting of water into oxygen and hydrogen is one of the most promising strategies to fulfill the future need for energy in a sustainable way. Photo-electrochemical cells (PECs) are attractive in this respect because the evolution of oxygen and hydrogen occurs at the physically separated anode and cathode, which simplifies the isolation of the gasses. Although several PECs have been reported that split water using inorganic light-harvesting materials (e.g., a-Si, $BiVO_4$, $GaInP_2$), the tuning of the bandgaps and band edges of these materials remains difficult and generally the stability of devices in water is poor.[1]

Dye-sensitized photo-electrochemical cells (DS-PECs) use molecular dye molecules as light-harvesting compounds. The absorbance, redox properties, and stability of these dye molecules can be optimized by synthetic modification, which is a major advantage for the optimization of DS-PECs. In DS-PECs, typically, a wide-band-gap semiconductor material is coated with dye molecules that are also coupled to a catalyst that performs the chemical transformation. Initially, in analogy to dye-sensitized solar cell research, DS-PEC research focused mainly on the development of a photoactive anode for water oxidation using Pt as the catalytic cathode for proton reduction.[2] Although light-driven proton reduction on a solid support has been reported,[3] only a few examples elaborate on the preparation of a photoactive cathode for proton reduction using NiO as the semiconductor material.[4]

Remarkably, no examples exist of the use of one of the fastest molecular proton-reduction catalysts (PRC), a Ni-DuBois-type PRC,[5] on a NiO electrode. In 2012, Li et al. described for the first time visible-light-driven hydrogen generation using an organic dye-modified NiO cathode in combination with a molecular Cobaloxime PRC.[6] In this system, the photocurrent decreased rapidly upon irradiation, which is assigned to either the decomposition of the catalyst or the leaching of the catalyst into solution. To improve catalyst binding, Ji et al. reported a photocathode in which a Ru-dye molecule is anchored on NiO and to the Cobaloxime catalyst through a supramolecular interaction.[7] With this system, the photocurrent was stable for several hours. Sun et al. combined these photocathodes for the first time with a photoanode that formed the first DS-PEC that could split water in a two-electrode setup.[8]

Herein, we report the construction of a NiO photocathode modified with an organic dye molecule and a Ni-DuBois-type PRC to form a new Ni-based photoelectrode.

[a] Dr. B. van den Bosch, Prof. Dr. J. N. H. Reek, Dr. R. J. Detz
Van't Hoff Institute for Molecular Sciences
University of Amsterdam
Science Park 904
1098 XH Amsterdam (The Netherlands)
E-mail: j.n.h.reek@uva.nl
r.j.detz@uva.nl

[b] J. A. Rombouts, Prof. Dr. R. V. A. Orru
Division of Organic Chemistry
Vrije Universiteit Amsterdam
De Boelelaan 1083a
1081 HV Amsterdam (The Netherlands)

Supporting Information and the ORCID identification number(s) for the author(s) of this article can be found under http://dx.doi.org/10.1002/cctc.201600025.

Results and Discussion

Electrode design

As demonstrated previously for p-type dye-sensitized solar cells (DSSC),[9] NiO is also a promising wide-bandgap semiconductor material for photocathode preparation for DS-PECs. The valence band (VB) potential energy of around 0.68 V vs. the normal hydrogen electrode (NHE; at pH 2)[10] determines the maximum reduction potential of the excited state of the dye to allow the quenching of the excited dye molecule (Figure 1).

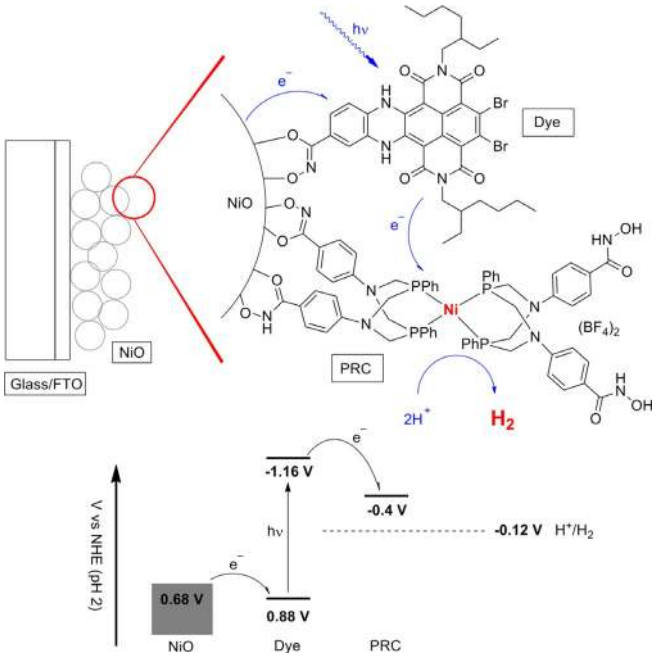

Figure 1. Schematic representation of the design parameters for the construction of a NiO-photocathode modified with an organic dye molecule and a Ni-DuBois-type PRC.

In addition, the reduced dye molecule should be able to reduce the PRC. For this purpose, a naphthalene diimide (NDI) scaffold was chosen as the core of our organic dye molecule. These NDIs have a typical HOMO level of 0.88 V vs. NHE.[11] This should make the quenching of the excited state of the dye by NiO possible. The reduction potential of the dye (−1.16 V vs. NHE) is sufficient to drive a Ni-DuBois-type PRC, which is reported to be active at a low overpotential in water.[3a,12]

A co-immobilization strategy is sought to simplify the synthetic scheme as the dye and catalyst can be prepared separately. The same approach was used to prepare the NiO-based photocathodes reported previously[7,8] and, moreover, to make photoanodes for water oxidation.[13] These studies already demonstrated that the choice of the anchoring group[14] and the distance[15] between the anchored components is very important for the electrode performance. To achieve a strong binding of the molecules to the NiO surface, hydroxamic acids were chosen as anchoring groups, which have been reported to bind very strongly to metal oxide surfaces.[14d]

Catalyst in solution

First, Ni complex **1** (Ni-**1**) was synthesized and studied by electrochemistry in solution. The cyclic voltammogram of Ni-**1** in CH_3CN/MeOH (4:1) displays one irreversible reduction at −0.9 V (vs. ferrocene/ferrocenium; Fc/Fc^+), which is ascribed to the Ni^{II}/Ni^{I} redox couple. This is in contrast to most reported bisdiphosphine nickel PRCs, which have two consecutive reversible reduction waves that correspond to the Ni^{II}/Ni^{I} and Ni^{I}/Ni^{0} redox couples.[16]

The irreversibility of the reduction and the absence of a second reduction might be caused by the poor solubility of the one-electron reduced species. A similar observation was reported for a bisdiphosphine nickel complex functionalized with carboxylic acids.[17] The addition of protonated DMF (DMFH·OTf) renders a catalytic reduction wave around −0.8 V (vs. Fc/Fc^+) in the cyclic voltammogram (Figure 2), which is ascribed to catalytic proton reduction. This potential is expected to be sufficiently low to be driven by potentials at the level of the CB of TiO_2. In the following section the immobilization of Ni-**1** on a TiO_2 electrode is described.

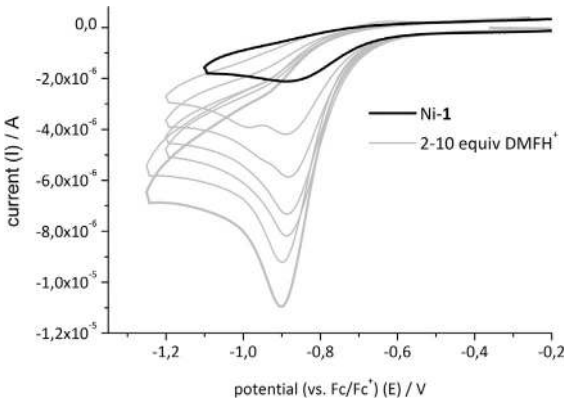

Figure 2. Cyclic voltammograms of a solution of Ni-**1** (black line) and a solution of Ni-**1** in the presence of increasing amounts of DMFH·OTf (2, 3, 5, 7, 8, and 10 equiv., gray lines). Conditions: 0.1 M Bu_4NPF_6 in CH_3CN/CH_3OH (2:1), mercury droplet working electrode, Ag wire counter electrode, scanning speed 0.1 $V s^{-1}$, referenced to Fc/Fc^+.

Catalyst on TiO_2

Ni-**1** is immobilized on fluorine-doped tin oxide (FTO) coated glass slides that bear a mesoporous layer (10 μm) of TiO_2 nanoparticles (20 nm). This allowed us to study this immobilized catalyst in the electrocatalytic reduction of protons in water.[18] After dip-coating the TiO_2-electrode in a solution of Ni-**1** (0.15 mM in CH_3CN/MeOH, 2:1) for 4 h, the now yellow-colored electrode was, after thorough washing, analyzed by using attenuated total reflectance (ATR) FTIR spectroscopy (see Supporting Information). Peaks that correspond to both Ni-**1** and TiO_2 appear in the ATR-FTIR spectrum of the Ni complex coated on the TiO_2 electrode (Ni-**1**@TiO_2) electrode. Furthermore, inductively coupled plasma optical emission spectroscopy (ICP-OES) of Ni (after the removal of the catalyst from the

surface in nitric acid) revealed that the catalyst loading was 76 nmol cm^{-2}.

The electrocatalytic activity was studied by submerging the Ni-**1**@TiO_2 electrode in an aqueous phosphate buffer (purged with N_2, 0.1 M, pH 2.1) in a three-electrode setup using a Pt coil as the counter electrode and a Ag/AgCl reference electrode. At a bias potential of −0.65 V, bubble formation was observed, and analysis of the headspace by GC proved the formation of hydrogen. After equilibration, a stable current density of −250 μA cm^{-2} was observed (Figure S4), which after half an hour decreased slowly to zero (after 1 h, 54 μL_{H_2} cm^{-2} was formed with a turnover number (TON) of 32). ATR-FTIR spectroscopy after electrocatalysis revealed that the catalyst was no longer bound to the electrode surface. The Faradaic efficiency was calculated to be 62% (after 1 h). This was lower than that described by others for a similar Ni catalyst in water at pH 4.5 (85%),[3a] which can be ascribed partly to the charging of the TiO_2.

The stability was improved by exchanging the phosphate buffer for a trifluoroacetate (TFA) buffer (0.1 M pH 2.1), although at the expense of a lower hydrogen production (after 1 h, 15 μL H_2 cm^{-2} was formed, TON = 9) and current density (−60 μA cm^{-2} after 1 h; Figure S5). Importantly, 50% of the initial activity was still observed after an impressive 3 h of electrocatalysis, although with a low Faraday efficiency (46%). These results were sufficiently convincing to proceed to the next step, which is the immobilization of Ni-**1** on NiO together with the organic dye molecule to construct the NiO photocathode.

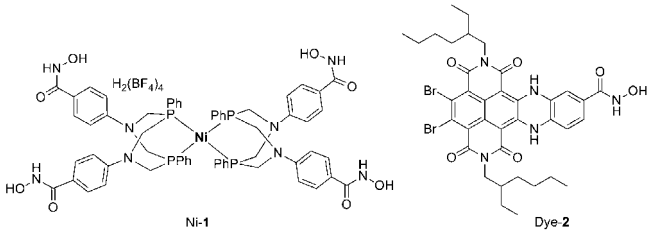

Catalyst and dye on NiO

The dye molecule **2** (Dye-**2**) was synthesized according to a slight modification of a literature procedure.[11,19] Next, Dye-**2** was anchored onto FTO-coated glass slides that bear a mesoporous layer of NiO nanoparticles by dipping the electrode into a solution of Dye-**2** in CH_2Cl_2 (0.6 mM). After washing, the obtained dark purple electrodes were analyzed by ATR-FTIR spectroscopy, which revealed several peaks that correspond to the dye molecule next to the peaks of NiO. The reduction potential of the dye on NiO was −1.16 V vs. NHE if measured in CH_2Cl_2 (Figure S8), no data could be obtained in acidic water because of a high background current. The immobilization of Ni-**1** on NiO was performed in a similar fashion as that of TiO_2 and gave also similar results as illustrated by the ATR-FTIR spectra (Figure 3 and Supporting Information). The co-immobilization of Ni-**1** with Dye-**2** was achieved by submerging the Ni-**1**@NiO electrode in a solution that contained Dye-**2**. Alternatively, the Dye-**2**@NiO electrode can be submerged in the solution that contained Ni-**1**. Slight differences in catalyst loading were measured: 4.3 nmol cm^{-2} for Dye-**2**@NiO+Ni-**1** and 5.2 nmol cm^{-2} for Ni-**1**@NiO+Dye-**2** (ICP analysis of phosphorus, see also Supporting Information). The ATR-FTIR spectrum of the Ni-**1**@NiO+Dye-**2** electrode (the order indicates the immobilization steps, for example, first immobilization of the complex followed by immobilization of the dye gives: Ni-**1**@NiO+Dye-**2**) shows the indicative ν(C=O) signals of the hydroxamic acids. The peaks around $\tilde{\nu}$ = 1603 cm^{-1} (indicated with ●) correspond to the C=O bond of the hydroxamate of the catalyst. The peaks at $\tilde{\nu}$ = 1580 cm^{-1} (indicated with ★) correspond to the C=O bond of the hydroxamate of the photosensitizer. This shows clearly that various ratios of dye and catalyst can be obtained by changing the loading conditions.

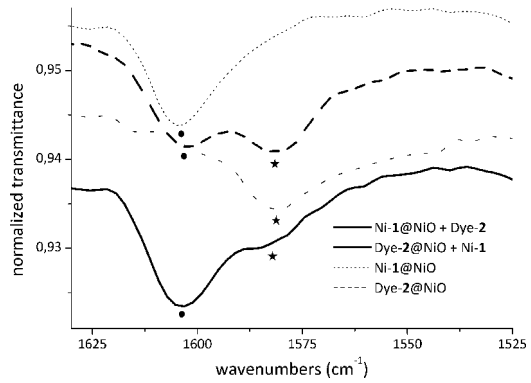

Figure 3. ATR-FTIR spectra of Ni-**1**@NiO+Dye-**2**, Dye-**2**@NiO+Ni-**1**, Ni-**1**@NiO, and Dye-**2**@NiO. The order indicates the steps of immobilization, for example, first immobilization of complex, followed by immobilization of the dye is Ni-**1**@NiO+Dye-**2**.

The functionalized electrodes were further characterized by using UV/Vis spectroscopy with integrated-sphere diffuse reflectance technology (Figure 4). The absorption of the immobilized Dye-**2** was observed clearly, which indicates successful immobilization. The relative intensity of the two major absorptions was changed upon immobilization. In CH_2Cl_2, the absorption at λ = 599 nm was more intense than that at λ = 552 nm. After binding on the NiO surface, the absorption at λ = 650 nm became more intense than that at λ = 615 nm. This change in the shape of the absorption spectrum is indicative of aggrega-

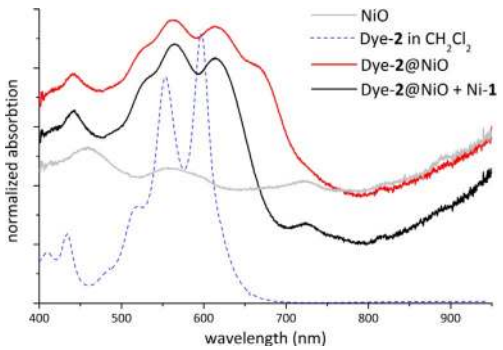

Figure 4. Reflectance UV/Vis spectra of NiO, Dye-**2**@NiO, and Dye-**2**@NiO+Ni-**1** and UV/Vis spectrum of Dye-**2** in CH_2Cl_2.

tion (or excimer formation), which is reported for various perylene diimide derivatives in solution.[20]

Furthermore, after the immobilization of Dye-**2**, the absorption was broadened dramatically compared to that of the dye in solution, and a redshift of all the maxima in the absorption spectra was observed. These two phenomena have been reported previously for the immobilization of other dyes on NiO and are ascribed to the coupling of the PS to NiO.[21] The broadening of the absorptions is more profound with the Dye-**2**@NiO electrodes than for the Dye-**2**@NiO+Ni-**1** electrode. In the latter, the co-immobilization of Ni-**1** probably separates the dye molecules, which thereby reduces aggregation. This suggests that the redshift and broadening of the absorptions and the change in the band shape is caused mainly by the aggregation of Dye-**2** and to a lesser extent by the coupling of the dye with NiO.

Additionally, the emission of the immobilized Dye-**2** after excitation at $\lambda = 565$ nm is redshifted and strongly broadened compared to that of Dye-**2** in CH_2Cl_2, which indicates aggregation (Figure 5). To our surprise, the emission of Dye-**2**@NiO+Ni-**1** is much higher than that of Dye-**2**@NiO.[22] An explanation for the increase in emission for the Dye-**2**@NiO+Ni-**1** electrode is that aggregation of the dye in the Dye-**2**@NiO electrode has a detrimental effect on the fluorescence. Unfortunately, because the quantum yield of the immobilized dye could not be determined, the percentage of dye that emits fluorescence is unknown, and the expected fluorescence quenching by hole injection into the NiO or electron transfer to the catalyst cannot be quantified in this way. Moreover, the dye is not quenched fully by hole injection as emission was still observed.

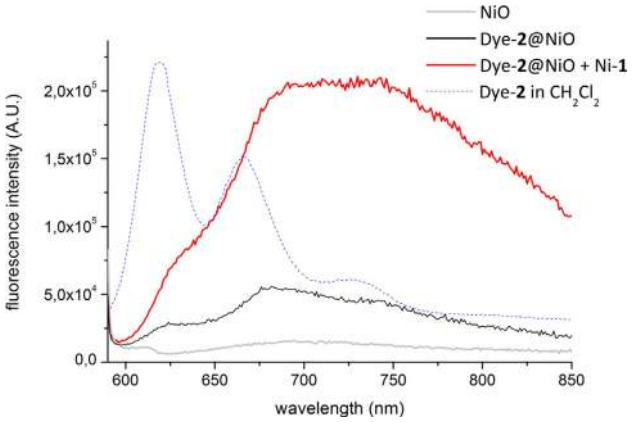

Figure 5. Fluorescence spectra (solid-state reflectance) of NiO, Dye-**2**@NiO, Dye-**2**@NiO+Ni-**1**, and (in solution) Dye-**2** in CH_2Cl_2.

Based on the results of ATR-FTIR, fluorescence, and reflectance UV/Vis spectroscopy, we conclude that both the dye and catalyst were immobilized successfully and co-immobilized on the NiO surface. Both the absorption and emission spectra of Dye-**2** changed upon immobilization. This means that the excited state energy of the immobilized dye also deviates from the excited state energy in solution. In the following section, we describe the electrochemical experiments that were conducted to see if the energy levels of the immobilized components are still properly aligned for electron transfer to take place.

Photo-electrochemistry

Linear sweep voltammetry measurements were performed with the NiO and the Dye-**2**@NiO electrodes as the working electrodes. We scanned the NiO electrodes and the Dye-**2**@NiO electrodes oxidatively in acetate buffer pH 4.7, while shielding them from light, and practically no current was observed between −0.2 and 0.15 V. Upon shining light on the NiO electrode no increase in current was observed, whereas shining light on the Dye-**2**@NiO electrode resulted in a photocurrent of $-40\ \mu A\,cm^{-2}$ (Figure S11). This current arises most probably from the reduction of oxygen by the reduced dye molecule as almost no photocurrent was observed under oxygen-free conditions (Figure S12). Importantly, this indicates that the VB of NiO is properly aligned with the reduction potential of the excited dye and that photoinduced hole injection into the NiO and hole transport through the nickel oxide occurs upon the excitation of Dye-**2**. The gradual increase in current at 0.15 V is ascribed to oxidation of the valence band of NiO. Furthermore, we used amperometry at a bias voltage of −0.1 V vs. Ag/AgCl in phosphate buffer pH 2, to measure that the Dye-**2**@NiO electrode gave a photocurrent of $-12\ \mu A\,cm^{-2}$ during two consecutive light on/off cycles (Figure 6) without any decrease in photocurrent, which indicates that the system is stable under the applied conditions. Similar observations were made if we used sodium acetate buffer at pH 4.7 (Figure S13).

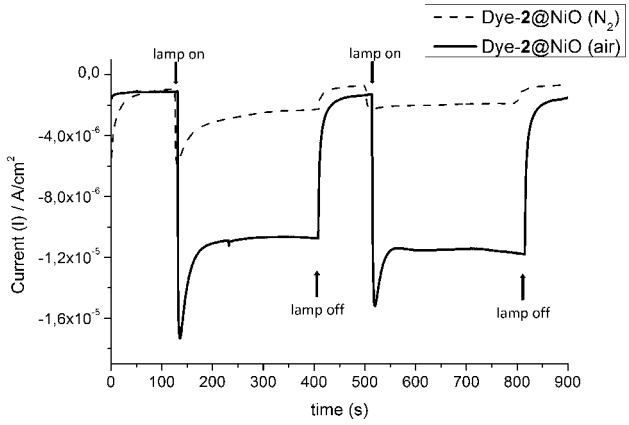

Figure 6. Amperometry of the Dye-**2**@NiO electrode in air (solid line) and flushed with N_2 (dotted line). Conditions: 0.1 M phosphate buffer pH 2, Pt counter electrode, leak-free Ag/AgCl reference electrode, AM1.5G solar simulation, 100 $mW\,cm^{-2}$ with 408 nm longpass filter, bias potential of −0.1 V vs. Ag/AgCl.

To see if photoinduced electron transfer can also take place from Dye-**2** to the Ni-**1** PRC, photocurrent measurements under anaerobic conditions were performed with Ni-**1** dissolved in a mixture of methanol/acetonitrile (1:1). In the first attempts, the photocurrent was not stable and decreased rapidly (a few

minutes) because of the replacement of the dye molecules by the catalyst, which was observed by ATR-FTIR spectroscopy. The experiment was repeated in acetonitrile using Ni-**3**,[16] which lacks the hydroxamic acid binding moieties. Now a stable photocurrent was observed for several minutes during amperometry. The current increased if we increased the concentration of Ni-**3**, which demonstrates that Ni-**3** accepts electrons from the reduced dye and acts as a redox mediator (Figure 7). A similar electron-transfer chain from NiO to the catalyst was also observed by Odobel et al.[4b]

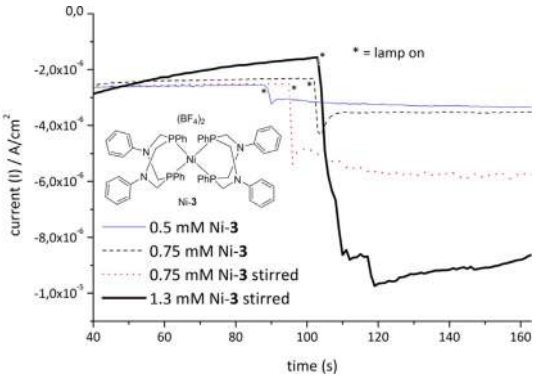

Figure 7. Amperometry of the Dye-**2**@NiO working electrode of various concentrations of Ni-**3** in CH_3CN purged initially with N_2. Conditions: 500 W XeHg lamp with 470 nm longpass filter, Pt coil as counter electrode, bias potential of −0.1 V vs. Ag/AgCl.

Photocatalysis

As we knew that all of the single-electron-transfer steps can occur, the photocatalytic properties of the photocathodes were evaluated in a standard three-electrode setup, with Ag/AgCl as the reference electrode and a Pt coil as the counter electrode. The irradiation of both the Dye-**2**@NiO+Ni-**1** and the Ni-**1**@NiO+Dye-**2** electrodes with light ($\lambda > 470$ nm) in phosphate buffer (pH 2.1) with a bias potential of −0.1 V did not lead to any photocurrent, and headspace analysis by GC did not reveal the formation of hydrogen gas. Unfortunately, also in experiments in which we used a sodium acetate buffer (pH 4.7) or 10 mM $DMFH^+$ in acetonitrile no observable photocurrent or hydrogen formation was observed.

The co-immobilization strategy allows the aggregation of the dye (or catalyst) molecules with each other, as was indicated by UV/Vis and fluorescence spectroscopy on the electrodes, instead of the formation of a homogeneous mixture of the molecules on the surface. This aggregation can prevent efficient electron transfer between reduced dye molecules and catalysts. Before the reduction of the catalyst takes place, a recombination event may occur because of electron injection from the reduced dye back into the NiO, which can explain the lack of photocatalytic activity.[23] Another possibility is that the second reduction of the co-immobilized Ni-**1** does not happen, which thus prevents photocatalysis in these cathodes. This can be explained by slow electron delivery to lead to fast recombination from the reduced catalyst to the oxidized NiO[3c] or by the instability of the catalyst after the first reduction to prevent the final step to achieve proton reduction.

Currently, our research focuses on how to achieve light-driven proton reduction on surfaces by slowing down recombination processes and improving catalyst activity and stability. To avoid aggregation issues, strategies are conducted to couple the catalyst to the dye molecules and prepare dyad structures, which can be immobilized in the assembled form.

Conclusions

Proton-reduction catalyst Ni-**1** could be attached to TiO_2 and was found to be a good electrocatalyst in aqueous solution (pH 2.1) to give a stable current of $-250\ \mu A\,cm^{-2}$ (overpotential of ≈300 mV). The catalyst could also be immobilized together with Dye-**2** on NiO electrodes to construct a Ni-based photocathode. It was shown that electron transfer from the NiO to the dye molecule and from the dye to the catalyst can occur upon light irradiation. Unfortunately, the electrodes are not photocatalytically active under irradiation in various acidic conditions upon application of a bias voltage of −0.1 V vs. Ag/AgCl. Possible bottlenecks that prevent photocatalytic proton reduction are poor electron transfer because of the aggregation of the molecules on the surface, charge recombination from the catalyst to the NiO, or the instability of Ni-**1** after the first reduction.

Experimental Section

Synthesis of Ni-1

Synthesis of 4-amino-*N*-hydroxybenzamide: NaOH (3.2 g, 80 mmol) and $NH_2OH{\cdot}HCl$ (2.78 g, 40 mmol) were dissolved in water (50 mL). Methyl 4-aminobenzoate (2.00 g, 13 mmol) dissolved in CH_3OH (30 mL) was added. This mixture was stirred at RT for 2 days, after which it was neutralized to pH 7 with 6 M HCl. The resulting solution was extracted with ethyl acetate (3×40 mL). The combined organic layers were dried over $MgSO_4$ and concentrated till some white precipitate was formed. This solution was placed at 4 °C overnight. The resulting white precipitate was collected by filtration and dried in vacuo. Yield: 54%. ^{1}H NMR ([D_6]DMSO, 298 K): $\delta = 10.75$ (br s, 1H), 8.67 (br s, 1H), 7.47 (d, $J = 8.6$ Hz, 2H), 6.53 (d, $J = 8.6$ Hz), 5.62 ppm (br s).

Synthesis of the ligand: Phenylphosphine (145 μL, 1.3 mmol) and formaldehyde (purged with N_2, 35% in water, 235 μL, 2.9 mmol) were heated to reflux in ethanol (5 mL; purged with N_2) for 18 h, after which all volatiles were removed in vacuo. The resulting white oil was dissolved in ethanol (5 mL; purged with N_2) and 4-amino-*N*-hydroxybenzamide (200 mg, 1.3 mmol) dissolved in water (7 mL; purged with N_2) with heating was added to the solution. The mixture was heated to reflux for 18 h. Another portion of 4-amino-*N*-hydroxybenzamide (100 mg, 0.66 mmol) dissolved in water with heating (3 mL; purged with N_2) was added to the solution and the mixture was heated to reflux for another hour to give full conversion (followed by ^{31}P NMR spectroscopy). The resulting white precipitate was collected by filtration over a glass filter, washed with water, and the white solid dried in vacuo. Yield: 54%. ^{1}H NMR ([D_6]DMSO, 25 °C) peaks of the major (83%) compound (see also Supporting Information) $\delta = 10.81$ (s, 2H), 8.74 (s, 2H), 7.72 (m, 4H), 7.58 (d, $J = 8.9$ Hz, 4H), 7.54 (m, 4H), 7.44 (m, 2H),

6.71 (d, $J=8.9$ Hz, 2H), 4.64 (m, 4H), 4.20 ppm (m, 4H); ^{31}P NMR ([D$_6$]DMSO, 25 °C): $\delta=-49.5$ ppm (s); IR: $\tilde{\nu}=1600$ (s), 1481 (s), 1454, 1434, 1383, 1333, 1307, 1250, 1211 (s), 1147 (s), 1025, 976, 896, 815, 751 (s), 692 (s), 602, 518, 469, 416 cm^{-1}; HRMS (ESI): *m/z*: calcd for $[C_{30}H_{30}N_4O_4P_2Na]^+$: 595.1640; found: 595.1603.

Synthesis of Ni-1: The ligand (44 mg, 0.076 mmol) and Ni(BF$_4$)·6 CH$_3$CN (18 mg, 0.038 mmol) were heated in CH$_3$CN (6 mL) at 50 °C. After 1 h, CH$_3$OH (1.5 mL) was added, and the red/white suspension was heated to reflux for 1.5 h. At this point, a solution of HBF$_4$·ether (5.5 μL in 1 mL CH$_3$CN) was added, and the mixture was stirred for 1 h upon which it turned bright red and the white precipitate had almost disappeared. After filtration and evaporation of the solvent a red solid was obtained, which was dried in vacuo (50 mg). Yield ($C_{60}H_{62}B_4F_{16}N_8NiO_8P_4$): 85%. ^{1}H NMR (300 MHz, CH$_3$CN-d$_3$, 25 °C): $\delta=12.39$ (br s), 7.83 (d, $J=8.5$ Hz, 8H), 7.55 (m, 6H), 7.30 (br m, 22H), 4.38 (d, $J=14.3$ Hz, 8H), 4.15 ppm (br d, $J=14.3$ Hz, 8H); ^{13}C NMR (300 MHz, [D$_3$]CH$_3$CN, 25 °C): 161.8, 154.9 (t, $J=4$ Hz),132.2, 130.9, 130.0, 129.4, 124.5 (t, $J=13$ Hz), 113.5, 49.8 ppm (very br); ^{31}P NMR (300 MHz, [D$_3$]CH$_3$CN, 25 °C): $\delta=-0.5$ ppm (s); IR: $\tilde{\nu}=1602$ (s), 1523, 1479 (s), 1436, 1417, 1393, 1200, 1056 (br s), 959, 878, 830, 738, 689, 518, 476 cm^{-1}; HRMS (ESI): *m/z*: calcd for $[C_{60}H_{59}N_8NiO_8P_4]^+$: 1201.2760; found: 1201.2846.

Synthesis of Dye-2

Synthesis of 3,4-diaminobenzene hydroxamic acid:[24] Methyl 3,4-diaminobenzoate (1.66 g, 10 mmol) was dissolved in dioxane (35 mL). Hydroxylamine hydrochloride (2.08 g, 30 mmol) and NaOH (2.40 g, 10 equiv., 100 mmol) in degassed water (15 mL) was added to this solution under stirring. After stirring at RT for 4 days, all volatiles are removed in vacuo. The reaction mixture was neutralized to a pH of approximately 7 through the cautious addition of concentrated HCl and stored at +4 °C to precipitate the product as brown needles. The obtained solid was collected by filtration, washed with a minimal volume of cold MeOH, and dried in vacuo. Yield 784 mg (47%). M.p.: 172–177 °C (decomp); ^{1}H NMR (500 MHz, DMSO, 25 °C): $\delta=10.64$ (s, 1H), 8.56 (s, 1H), 6.97 (s, 1H), 6.85 (d, 1H, $^3J=8.0$ Hz), 6.44 (d, 1H, $^3J=8.0$ Hz), 4.94 (s, 2H), 4.56 ppm (s, 2H); ^{13}C NMR (125.8 MHz, DMSO, 20 °C): $\delta=165.8$, 138.4, 134.0, 120.9, 116.6, 113.5, 112.8 ppm; IR: $\tilde{\nu}=3301$, 3175, 1630, 1585, 1506, 1464, 1523, 1311, 1281, 1236, 1126, 1080, 1032, 892, 841, 810, 770, 731, 554, 515, 447 cm^{-1}; HRMS (ESI): *m/z*: calcd for $[C_7H_{10}N_3O_2]^+$: 168.0773; found: 168.0772.

Synthesis of 4,5,9,10-tetrabromonaphthalene di(2-ethylhexyl)imide: 2-Ethylhexylamine (7.5 mL, 45 mmol) was added to degassed glacial acetic acid (100 mL). 2,3,6,7-Tetrabromonaphtalene dianhydride (8.4 g, 15 mmol) was added, and the mixture was heated to reflux with a sand bath at 150 °C. The initially turbid yellow suspension turned into a clear, dark brown solution after 10 min of reflux, upon which the reaction vessel was cooled in an ice bath. Immediate dilution with water (500 mL) water at RT precipitated a bright yellow solid, which was triturated with water, aqueous NaHCO$_3$, and cyclohexane on a Buchner filter. Vacuum drying at RT gave a bright yellow solid (9.7 g), which could not be analyzed satisfactorily by using NMR spectroscopy or MS. The yellow solid was dissolved in degassed, distilled toluene (50 mL) and heated to reflux. After 10 min, PBr$_3$ (3.3 mL, 35 mmol) was added dropwise with a syringe. 25 min after addition, the reaction mixture was cooled and diluted under vigorous stirring with NaHCO$_3$ (500 mL) to quench excess PBr$_3$. The aqueous phase was extracted with 3×200 mL CH$_2$Cl$_2$. The combined organic layers were dried over MgSO$_4$ and concentrated in vacuo, after which column chromatography (alumina; eluent system 1:1 pentane/CHCl$_3$) was performed to yield the product as an orange-yellow solid. Yield: 8%. NMR spectroscopic data of the compound is identical to literature values.[25] M.p.: 233–235 °C (decomp); TLC (CH$_2$Cl$_2$): $R_f=0.7$, yellow spot; ^{1}H NMR (500 MHz, CDCl$_3$, 25 °C): $\delta=4.19$ (d, 4H, $^3J=7.5$ Hz), 1.94 (m, 2H), 1.28–1.38 (m, 16H), 0.94 (t, 6H, $^3J=7.5$ Hz), 0.88 ppm (t, 6H, $^3J=6.3$ Hz); ^{13}C NMR (125.8 MHz, CDCl$_3$, 20 °C): $\delta=160.3$, 135.40, 126.5, 125.8, 46.3, 37.8, 30.6, 28.5, 23.9, 23.1, 14.1, 10.6 ppm; ATR-FTIR: $\tilde{\nu}=2959$, 2924, 2910, 2855, 1709, 1661, 1585, 1458, 1435, 1406, 1373, 1308, 1283, 1192, 1155, 1139, 721, 582, 463 cm^{-1}.

Synthesis of Dye-2: To a glass 20 mL microwave reactor 4,5,9,10-tetrabromonaphthalene di(2-ethylhexyl)imide (130 mg, 0.16 mmol, 1.0 equiv.) and 3,4-diaminobenzene hydroxamic acid (108 mg, 0.64 mmol, 4.0 equiv) were added, together with degassed DMF (10 mL). The yellow suspension was degassed for 5 min with a stream of N$_2$, and capped with a Teflon-lined stopper, after which the vessel was heated using microwave irradiation for 30 min at 85 °C. The blue reaction mixture was cooled and poured into CH$_2$Cl$_2$. The organic layer was extracted with saturated aqueous NaHCO$_3$, aqueous HCl (1 M), and water. The organic layer was dried over Na$_2$SO$_4$ and concentrated in vacuo. Column chromatography (SiO$_2$, 100% CH$_2$Cl$_2$ to 9:1 CH$_2$Cl$_2$/HOAc) afforded the product as a dark blue solid. Yield 66.6 mg (51%). Poor solubility precluded NMR spectroscopy of this material. M.p.: >300 °C; IR: $\tilde{\nu}=2959$, 2926, 2856, 1693, 1628, 1582, 1501, 1456, 1308, 1248, 1231, 1132, 1030 cm^{-1}; HRMS (coldspray): *m/z*: calcd for $[C_{37}H_{42}Br_2N_5O_6]^+$: 812.14814; found: 812.14858; elemental analysis calcd for $C_{37}H_{41}Br_2N_5O_6$ (MW = 811.57): C 54.76, H 5.09, N 8.63; found: C 54.47, H 5.28, N 8.54.

Acknowledgements

This work is part of the ECHO research programme, which is (partly) financed by the Netherlands Organisation for Scientific Research (NWO). This project was carried out within the research programme of BioSolar Cells, co-financed by the Dutch Ministry of Economic Affairs. Z. Abiri is acknowledged for the synthetic efforts contributing to this work. We thank Prof. Dr. A. M. Brouwer and Dr. R. M. Williams for fruitful discussions, E. Zuidinga for mass analysis, and L. de Lange for ICP analysis.

Keywords: electrochemistry · dyes/pigments · hydrogen · nickel · photochemistry

[1] a) F. E. Osterloh, *Chem. Soc. Rev.* **2013**, *42*, 2294–2320; b) K. Maeda, K. Domen, *J. Phys. Chem. Lett.* **2010**, *1*, 2655–2661; c) K. Sun, S. Shen, Y. Liang, P. E. Burrows, S. S. Mao, D. Wang, *Chem. Rev.* **2014**, *114*, 8662–8719; d) M. G. Walter, E. L. Warren, J. R. McKone, S. W. Boettcher, Q. Mi, E. A. Santori, N. S. Lewis, *Chem. Rev.* **2010**, *110*, 6446–6473.

[2] For a recent review, see: Z. Yu, F. Li, L. Sun, *Energy Environ. Sci.* **2015**, *8*, 760–775.

[3] a) M. A. Gross, A. Reynal, J. R. Durrant, E. Reisner, *J. Am. Chem. Soc.* **2014**, *136*, 356–366; b) F. Lakadamyali, A. Reynal, M. Kato, J. R. Durrant, E. Reisner, *Chem. Eur. J.* **2012**, *18*, 15464–15475; c) J. M. Gardner, M. Beyler, M. Karnahl, S. Tschierlei, S. Ott, L. Hammarström, *J. Am. Chem. Soc.* **2012**, *134*, 19322–19325; d) E. Reisner, J. C. Fontecilla-Camps, F. A. Armstrong, *Chem. Commun.* **2009**, 550–552.

[4] a) L. Tong, A. Iwase, A. Nattestad, U. Bach, M. Weidelener, G. Götz, A. Mishra, P. Bäuerle, R. Amal, G. G. Wallace, A. J. Mozer, *Energy Environ. Sci.*

2012, *5*, 9472 – 9475; b) C. E. Castillo, M. Gennari, T. Stoll, J. Fortage, A. Deronzier, M.-N. Collomb, M. Sandroni, F. Légalité, E. Blart, Y. Pellegrin, C. Delacote, M. Boujtita, F. Odobel, P. Rannou, S. Sadki, *J. Phys. Chem. C* **2015**, *119*, 5806 – 5818.

[5] a) M. L. Helm, M. P. Stewart, R. M. Bullock, M. R. DuBois, D. L. DuBois, *Science* **2011**, *333*, 863 – 866; b) A. Dutta, D. L. DuBois, J. A. S. Roberts, W. J. Shaw, *Proc. Natl. Acad. Sci. USA* **2014**, *111*, 16286 – 16291.

[6] L. Li, L. Duan, F. Wen, C. Li, M. Wang, A. Hagfeldt, L. Sun, *Chem. Commun.* **2012**, *48*, 988 – 990.

[7] Z. Ji, M. He, Z. Huang, U. Ozkan, Y. Wu, *J. Am. Chem. Soc.* **2013**, *135*, 11696 – 11699.

[8] a) K. Fan, F. Li, L. Wang, Q. Daniel, E. Gabrielsson, L. Sun, *Phys. Chem. Chem. Phys.* **2014**, *16*, 25234 – 25240; b) F. Li, K. Fan, B. Xu, E. Gabrielsson, Q. Daniel, L. Li, L. Sun, *J. Am. Chem. Soc.* **2015**, *137*, 9153 – 9159.

[9] a) F. Odobel, L. Le Pleux, Y. Pellegrin, E. Blart, *Acc. Chem. Res.* **2010**, *43*, 1063 – 1071; b) F. Odobel, Y. Pellegrin, E. A. Gibson, A. Hagfeldt, A. L. Smeigh, L. Hammarström, *Coord. Chem. Rev.* **2012**, *256*, 2414 – 2423.

[10] G. Boschloo, A. Hagfeldt, *J. Phys. Chem. B* **2001**, *105*, 3039 – 3044.

[11] Q. Ye, J. Chang, K. Huang, X. Shi, J. Wu, C. Chi, *Org. Lett.* **2013**, *15*, 1194 – 1197.

[12] D. W. Wakerley, M. A. Gross, E. Reisner, *Chem. Commun.* **2014**, *50*, 15995 – 15998.

[13] D. L. Ashford, M. K. Gish, A. K. Vannucci, M. K. Brennaman, J. L. Templeton, J. M. Papanikolas, T. J. Meyer, *Chem. Rev.* **2015**, *115*, 13006 – 13049.

[14] a) Y. Gao, X. Ding, J. Liu, L. Wang, Z. Lu, L. Li, L. Sun, *J. Am. Chem. Soc.* **2013**, *135*, 4219 – 4222; b) W. R. McNamara, R. C. Snoeberger, G. Li, J. M. Schleicher, C. W. Cady, M. Poyatos, C. A. Schmuttenmaer, R. H. Crabtree, G. W. Brudvig, V. S. Batista, *J. Am. Chem. Soc.* **2008**, *130*, 14329 – 14338; c) W. J. Youngblood, S. A. Lee, Y. Kobayashi, E. A. Hernandez-Pagan, P. G. Hoertz, T. A. Moore, A. L. Moore, D. Gust, T. E. Mallouk, *J. Am. Chem. Soc.* **2009**, *131*, 926 – 927; d) W. R. McNamara, R. C. Snoeberger III, G. Li, C. Richter, L. J. Allen, R. L. Milot, C. A. Schmuttenmaer, R. H. Crabtree, G. W. Brudvig, V. S. Batista, *Energy Environ. Sci.* **2010**, *3*, 917 – 923.

[15] Y. Gao, L. Zhang, X. Ding, L. Sun, *Phys. Chem. Chem. Phys.* **2014**, *16*, 12008 – 12013.

[16] U. J. Kilgore, J. A. Roberts, D. H. Pool, A. M. Appel, M. P. Stewart, M. R. DuBois, W. G. Dougherty, W. S. Kassel, R. M. Bullock, D. L. DuBois, *J. Am. Chem. Soc.* **2011**, *133*, 5861 – 5872.

[17] A. Jain, S. Lense, J. C. Linehan, S. Raugei, H. Cho, D. L. DuBois, W. J. Shaw, *Inorg. Chem.* **2011**, *50*, 4073 – 4085.

[18] As a result of very poor solubility, Ni-**1** could not be studied by electrochemistry dissolved in water.

[19] J. A. Rombouts, J. Ravensbergen, R. N. Frese, J. T. M. Kennis, A. W. Ehlers, J. C. Slootweg, E. Ruijter, K. Lammertsma, R. V. A. Orru, *Chem. Eur. J.* **2014**, *20*, 10285 – 10291.

[20] a) C. Haines, M. Chen, K. P. Ghiggino, *Sol. Energy Mater. Sol. Cells* **2012**, *105*, 287 – 292; b) S. Asir, A. S. Demir, H. Icil, *Dyes Pigm.* **2010**, *84*, 1 – 13; c) C. Hippius, I. H. M. van Stokkum, E. Zangrando, R. M. Williams, M. Wykes, D. Beljonne, F. Würthner, *J. Phys. Chem. C* **2008**, *112*, 14626 – 14638; d) D. Veldman, S. M. A. Chopin, S. C. J. Meskers, M. M. Groeneveld, R. M. Williams, R. A. J. Janssen, *J. Phys. Chem. B* **2008**, *112*, 5846 – 5857; e) W. E. Ford, P. V. Kamat, *J. Phys. Chem.* **1987**, *91*, 6373 – 6380.

[21] a) C. J. Wood, K. C. D. Robson, P. I. P. Elliott, C. P. Berlinguette, E. A. Gibson, *RSC Adv.* **2014**, *4*, 5782 – 5791; b) J. He, H. Lindström, A. Hagfeldt, S. Lindquist, *J Phys Chem. B.* **1999**, *103*, 8940 – 8943; c) P. Qin, H. Zhu, T. Edvinsson, G. Boschloo, A. Hagfeldt, L. Sun, *J. Am. Chem. Soc.* **2008**, *130*, 8570 – 8571.

[22] The Ni-**1**@NiO electrode has a very small emission compared to Dye-**2**@NiO, and the blank NiO electrode practically does not emit under the applied conditions.

[23] L. D'Amario, L. J. Antila, B. P. Rimgard, G. Boschloo, L. Hammarström, *J. Phys. Chem. Lett.* **2015**, *6*, 779 – 783.

[24] O. Kreye, S. Wald, M. A. R. Meier, *Adv. Synth. Catal.* **2013**, *355*, 81 – 86.

[25] X. Gao, C. Di, Y. Hu, X. Yang, H. Fan, F. Zhang, Y. Liu, H. Li, D. Zhu, *J. Am. Chem. Soc.* **2010**, *132*, 3697 – 3699.

Received: January 8, 2016
Published online on February 23, 2016